Kinetics of Inhibition of β-Amyloid Aggregation by Transthyretin†

Lin Liu and Regina M. Murphy*

Department of Chemical and Biological Engineering, University of Wisconsin, 1415 Engineering Drive, Madison, Wisconsin 53706

Received September 5, 2006; Revised Manuscript Received October 27, 2006

ABSTRACT: Deposition of β-amyloid (Aβ) fibrils is an early event in the neurodegenerative processes associated with Alzheimer's disease. According to the "amyloid cascade" hypothesis, Aβ aggregation, and its subsequent deposition as fibrils, is the underlying cause of disease. Aβ is a proteolytic product of amyloid precursor protein (APP); several mutations in APP have been identified that are associated with early onset of disease. Transgenic mice overexpressing APP with the Swedish mutation develop numerous plaques but, surprisingly, lack the neurofibrillary tangles and neuronal loss characteristic of Alzheimer's disease, in apparent contradiction of the amyloid cascade hypothesis. However, recent studies suggest that coproduction of sAPPα, an alternative proteolytic product of APP, increases synthesis of transthyretin that, in turn, interacts directly with Aβ to inhibit its toxicity. Here we report results from biophysical analysis of Aβ aggregation kinetics in the presence of transthryetin. At substoichiometric ratios, transthyretin drastically decreased the rate of aggregation without affecting the fraction of Aβ in the aggregate pool. Detailed analysis of the data using a mathematical model demonstrated that the decrease in aggregation rate was due to both a decrease in the rate of elongation relative to the rate of initiation of filaments and a decrease in lateral association of filaments to fibrils. Tryptophan quenching data indicated that transthyretin binds weakly to Aβ, with an estimated apparent K_S of 2300 M^{-1}. Taken together, the data support a hypothesis wherein transthyretin preferentially binds to aggregated rather than monomeric Aβ and arrests further growth of the aggregates.

Alzheimer's disease (AD[1]) is the most prevalent form of age-associated dementia, characterized by extracellular senile plaques, intraneuronal neurofibrillary tangles, and widespread neuronal cell death. The main protein component of the senile plaques is β-amyloid (Aβ), deposited as fibrillar aggregates. According to the "amyloid cascade hypothesis", accumulation of Aβ fibrils is an early and essential event in the AD neurodegenerative process (*1*).

Aβ is generated when β- and γ-secretases cleave a large transmembrane protein, amyloid precursor protein, or APP (*2*). Alternative cleavage of APP by α-secretase generates sAPPα, a fragment that is not amyloidogenic and may be neuroprotective (*3*, *4*). The Swedish mutation of APP, APP_{Sw}, is associated with increased Aβ deposition and early onset Alzheimer's disease. Transgenic mice overexpressing APP_{Sw} develop numerous Aβ amyloid deposits (*5*), but lack the neurofibrillary tangles and neuronal cell loss characteristic of AD (*6*). These findings seemed to contradict the amyloid cascade hypothesis. However, Stein and Johnson hypothesized that the APP_{Sw} mice were mounting a neuroprotective response to Aβ expression (*7*). By DNA microarray experiments, they discovered that the mRNA of transthyretin (TTR), a transport protein abundant in blood and cerebrospinal fluid (CSF), was increased 30-fold in the hippocampus and 3-fold in the cerebellum in APP_{SW} mice compared to controls (*7*). Furthermore, they demonstrated that sAPPα induced the increase of TTR expression, and that anti-TTR antibody destroyed the protective effect of sAPPα against Aβ-induced cell death (*8*). Hence, their data suggest that APP_{Sw} mice produce high levels of both Aβ (product of the β- and γ-secretase cleavage of APP) and sAPPα (product of α-secretase cleavage of APP); the latter increases TTR production which in turn protects the cells from Aβ.

TTR, a 55 kDa homotetramer, is the major protein in CSF and is also found in human plasma, serving as the main transporter of thyroid hormones from the blood stream into CSF. In plasma, it is involved in transport of retinol-binding protein (*9*). TTR is stable at physiological pH, but readily aggregates into amyloid fibrils under acidic conditions; several mutants that form fibrils at neutral pH have been discovered (*10*). Amyloid deposits of both wild-type and mutant TTR are disease-associated: wild-type TTR fibrils are observed in late-onset systemic senile amyloidosis (*11*), while mutant TTR fibrils are linked to familial amyloid polyneuropathy (*12*).

Further evidence of a link between TTR, Aβ, and AD comes from several studies. TTR levels in CSF were lower in multi-infarct dementia (*13*) and AD (*14*, *15*) than in age-matched controls. Nicotine was found to enhance the biosynthesis of TTR in rats, which was postulated to account for the inverse association between cigarette smoking and

† This work was supported by Grant IIRG-05-13270 from the Alzheimer's Association.

* Corresponding author. (608) 262-1587. Fax: (608) 262-5434. E-mail: regina@engr.wisc.edu.

[1] Abbreviations: Aβ, beta-amyloid; AD, Alzheimer's disease; APP, amyloid precursor protein; APP_{sw}, Swedish mutation of APP; BSA, bovine serum albumin; CSF, cerebrospinal fluid; PBSA, phosphate-buffered saline with azide; SEC, size exclusion chromatography; SLS, static light scattering; TEM, transmission electron microscope; TTR, transthyretin.

10.1021/bi0618520 CCC: $33.50
Published on Web 12/19/2006

AD (*16*). Estrogen protection against AD was related to increased synthesis of TTR in the choroid plexus (*17*). Transgenic *Caenorhabditis elegans* nematodes expressing Aβ produced muscle-specific deposits immunoreactive with Aβ antibodies, but strains coexpressing Aβ and TTR showed a dramatic reduction in those deposits (*18*). Finally, several groups demonstrated directly that Aβ associates with TTR (*19*−*23*).

Taken together, these data have led to the hypothesis that Aβ is normally sequestered by TTR and that the failure of this sequestration contributes to development of AD (*19*, *20*). However, few details are known about the mechanism by which TTR inhibits aggregation of Aβ. In work reported here, we examined the size and morphology of Aβ aggregates, and the kinetics of Aβ aggregation, in the presence of TTR. Using a previously developed kinetic model of Aβ aggregation (*24*) to analyze the data, we identified the steps in the Aβ aggregation process that are influenced by TTR. The binding affinity of TTR to Aβ was also estimated.

MATERIALS AND METHODS

Sample Preparation. Molecular-biology-grade urea was purchased from Boehringer-Mannheim (Indianapolis, IN). All other chemicals were purchased from Sigma-Aldrich. PBSA (0.01 M Na_2HPO_4/NaH_2PO_4, 0.15 M NaCl, 0.02% w/v NaN_3, pH 7.4) was double filtered through 0.22 μm filters. 8 M urea was prepared in 10 mM glycine−NaOH buffer, pH 10, and then double filtered through 0.22 μm filters. Lyophilized Aβ(1−40) (AnaSpec, San Jose, CA), was dissolved at a concentration of 2.8 mM in the 8 M urea/glycine buffer. Urea dissolution was required to yield quantitatively reproducible results and to ensure a monomeric and unfolded initial state (*24*). TTR purified from human plasma (Sigma Aldrich, St. Louis, MO) was dissolved at 1 μM, 2 μM, or 3.3 μM in PBSA. Purity was checked by SDS−PAGE; the denatured protein ran as a monomer (14 kDa) (data not shown). A faint band (estimated at ∼1−2%) was detected at ∼35 kDa; the identity of this minor contaminant is unknown. The stock solution of Aβ was diluted 20-fold into filtered PBSA, or PBSA with TTR, to a final Aβ concentration of 140 μM. Samples were rapidly filtered through 0.45 μm filters directly into light-scattering cuvettes for light scattering, or microtubes for size exclusion chromatography (SEC). Residual urea was 0.4 M, and pH of the final solution was 7.4.

Transmission Electron Microscopy. Samples of Aβ alone or with 1 μM TTR, prepared as described above, were incubated for 4 days at room temperature, then stained with NanoW negative stain (Nanoprobes.com, Yaphank, NY) and placed on a pioloform coating grid support film (Ted Pella Inc., Redding, CA), and then analyzed by a Philips CM120 Transmission Electron Microscope (FEI Corp., Eindhoven, The Netherlands).

Size Exclusion Chromatography (SEC). Samples were analyzed with SEC using a precision column prepacked with Superdex 75 (Pharmacia, Piscataway, NJ) on a Pharmacia fast protein liquid chromatography system, as described previously (*24*). Mobile phase flow rate was set at 0.05 mL/min, and elution peaks were detected by absorbance at 280 nm. The mobile phase buffer was matched to the one used for dissolution of Aβ. The concentration of the nonaggregated portion of Aβ (monomer and dimer) was calculated from its peak area using an extinction coefficient of 0.3062 $(mg/mL)^{-1}$ cm^{-1} (*24*). BSA was used to calibrate the relationship between peak area and concentration: the concentration of a BSA solution was determined by absorbance at 280 nm using an extinction coefficient of 0.667 $(mg/mL)^{-1}$ cm^{-1}, and then a known volume was injected onto the column and the peak area determined. The TTR peak was collected and concentration was measured with the BCA assay (Pierce, Rockland, IL).

Laser Light Scattering. Cuvettes were placed in a bath of the index-matching solvent decahydronaphthalene, with the temperature controlled at 25 °C. Dynamic and static light scattering measurements were taken, using a Coherent (Santa Clara, CA) argon ion laser operated at 488 nm and a Malvern 4700c system (Southborough, MA), as described in more detail elsewhere (*25*). The earliest data points were collected approximately 10 min after sample preparation. The average scattered intensity I_S and the autocorrelation function were measured at 90° scattering angle repeatedly over a 20 h interval. Autocorrelation data were fitted to a third-order cumulants expression to determine the inverse *z*-average apparent hydrodynamic radius R_{hz}.

After 20 h, the average particle molecular mass, shape, and dimensions of the same samples were obtained by multiangle static light scattering (SLS) measurements using the same apparatus as described previously in detail (*25*). Briefly, the scattered light intensity at 24 angles from 20° to 135° was collected; each measurement was repeated five times and averaged. Average scattered intensity of the buffer was measured in the same manner and subtracted from the sample scattering intensity; the result was then normalized by using the scattering intensity of the reference solvent toluene to obtain the Rayleigh ratio $R_s(q)$ as a function of scattering vector $q = (4\pi n/\lambda_o)\sin(\theta/2)$ where n is the refractive index of the solvent, λ_0 is the wavelength of the incident beam in vacuum, and θ is the scattering angle. The data were plotted in the Zimm format, as $Kc/R_s(q)$ versus q^2, where $K = 4\pi^2n^2(dn/dc)^2/N_A\lambda_o^4$, c is the total protein concentration (g/mL), dn/dc is the *z*-averaged refractive index increment (assumed to be 0.145 mL/g and independent of aggregation state (*24*)), and N_A is Avogadro's number.

At $c \rightarrow 0$ and $q^2\langle R_g^2\rangle_z/3 \ll 1$,

$$\frac{Kc}{R_s(q)} = \frac{1}{M_w}\left[1 + \frac{q^2\langle R_g^2\rangle_z}{3}\right] \quad (1)$$

where M_w is the weight-averaged molecular weight and $\langle R_g^2\rangle_z$ is the *z*-averaged squared radius of gyration, which is very heavily weighted toward larger particles. We fit the scattering data at angles less than 50° ($q < 0.0145$ nm^{-1}) to eq 1 to obtain M_w and R_g $(=\sqrt{\langle R_g^2\rangle_z})$. This analysis neglects any second-virial coefficient correction.

At higher scattering angles and with larger particle sizes, the assumption that $q^2\langle R_g^2\rangle_z/3 \ll 1$ is no longer valid. Under these conditions,

$$\frac{R_s(q)}{Kc} = M_w P(q) \quad (2)$$

where $P(q)$, the particle scattering factor, is a complex function of particle shape and dimension. The Kratky plot,

in which $q^2R_s(q)/Kc = q^2M_wP(q)$ is plotted versus q, is a convenient means for monitoring morphology of particles with characteristic dimensions comparable to the wavelength of the incident beam (*26*). A smoothly rising plot with a plateau at intermediate q is typical of semiflexible linear chains, whereas a linear monotonic increase suggests stiff-rod structure. The semiflexible chain model describes a linear chain with total contour length L_c and Kuhn statistical segment length l_k (a measure of the stiffness of the chain, equal to two times the persistence length). $P(q)$ for semiflexible wormlike chains is

$$P(q) = \frac{2}{L_c^2}\int_0^{L_c}(L_c - t)\phi(t,l_k,q)\,dt \qquad (3)$$

where the function $\phi(t,l_k,q)$ has been described elsewhere (*27*). Aggregate size for Aβ alone and in the presence of 1 μM TTR was sufficiently large to justify use of eqs 2 and 3; M_w, L_c, and l_k were determined by nonlinear regression of eqs 2 and 3 to the multiangle scattering data using the parameter estimation software program ATHENA. R_g was calculated from L_c and l_k using

$$R_g = \sqrt{\frac{L_c l_k}{6} - \frac{l_k^2}{4} + \frac{l_k^3}{4L_c} - \frac{l_k^4}{8L_c^2}(1 - e^{-2L_c/l_k})} \qquad (4)$$

R_h was calculated from L_c and l_k using equations appropriate for semiflexible chains, as described elsewhere (*28*).

Kinetic Modeling. A kinetic model of Aβ aggregation has been described previously (*24*). This model was fitted to the measured quantities I_{90} and R_{hz} versus time, to compare Aβ aggregation rates in the absence and presence of TTR. The model postulates an evolving distribution of Aβ monomer, dimer, intermediates, filaments, and fibrils, and assumes that filaments and fibrils can be modeled as semiflexible chains. Filament diameter was assumed to be 4 nm, and l_k was determined from the multiangle scattering data (for Aβ alone and with 1 μM TTR), or was set equal to 180 nm (*24*). The best fit of the data to the model was obtained by nonlinear least-squares regression, using ATHENA software. The model and data fitting are described in detail elsewhere (*24*). As described further in the Results section, all parameter values were unchanged from those determined previously, except for model parameters associated with aggregate growth, i.e., filament initiation and elongation (k_p/k_n), fibril formation by lateral association (k_{la}), and fibril growth by end-to-end association ($\delta\varpi_{fib}$).

Tryptophan Fluorescence. TTR at 1 μM was mixed with Aβ at 21 μM, 42 μM, or 84 μM in double-filtered PBSA (pH = 7.4, 0.24 M residual urea). After incubation at room temperature for 1 h, samples were put in UV-permeable cuvettes, and fluorescence spectra were obtained with a QuantaMaster Series spectrofluorometer (PTI, Inc., Birmingham, NJ), with excitation at 290 nm and emission spectra recorded from 300 to 420 nm. The emission intensity values were scaled by setting the maximum emission intensity of 1 μM TTR alone to be unity. The data were analyzed using the Stern−Volmer equation,

$$\frac{F_0}{F} = 1 + K_S[Q] \qquad (5)$$

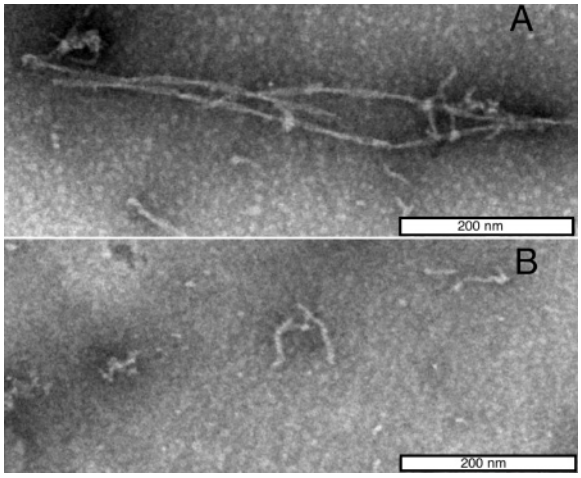

FIGURE 1: TEM image of Aβ (140 μM) without (A) and with (B) 1 μM TTR. Scale bars indicate 200 nm.

where F and F_0 are the maximum fluorescence intensity with and without quencher, respectively; [Q] is the concentration of quencher (Aβ); and K_S is the association constant between quencher and fluorophore. We evaluated F_0 and F at 339 nm and obtained K_S from linear regression. If the quenching is caused by dynamic collision between the quencher and fluorophore molecules, K_S is equal to the product of the biomolecular quenching constant k_q and the lifetime of the fluorophore without quencher τ_0. For tryptophan in proteins $\tau_0 \sim 10$ ns; in aqueous solution the maximum $k_q \sim 10^{10}$ M^{-1} s^{-1} (*29*), so the maximum value of K_S with dynamic quenching is $\sim$100 M^{-1}. If the measured K_S value is significantly greater than 100 M^{-1}, we assume the quenching results from formation of complexes rather than dynamic quenching.

RESULTS

Effect of TTR on Aβ Aggregate Size and Morphology. As observed in TEM images, Aβ alone formed typical amyloid fibrils, with diameters of $\sim$10 nm, lengths of 1 μm or more, and a characteristic twisted appearance (Figure 1A). Addition of 1 μM TTR to 140 μM Aβ noticeably reduced the number of large aggregates and significantly decreased the length of those aggregates that were observed, without gross changes in their linear morphology (Figure 1B).

Previously we observed that only a fraction of Aβ was incorporated into soluble aggregates under our experimental conditions, while some of the peptide remained unaggregated (*24*). To determine whether TTR affected the distribution of Aβ between aggregated and nonaggregated forms, solutions of Aβ and TTR alone or mixed together were analyzed by size exclusion chromatography (SEC). Representative chromatograms are shown in Figure 2. We have previously observed that Aβ aggregates tend to be captured either by the guard column or by adsorption to the main column (*24*); thus the major eluting species is the nonaggregated component. With Aβ, a single defined peak was observed eluting at $\sim$34 min. This peak was identified as monomer/dimer based on column calibration. From the peak area of eluted Aβ we calculated that 67 $\pm$ 3% of the peptide was not aggregated, consistent with previous reports (*24*). TTR alone eluted at $\sim$27 min, consistent with an expected molecular weight of 55 kDa. When mixtures of Aβ and TTR were

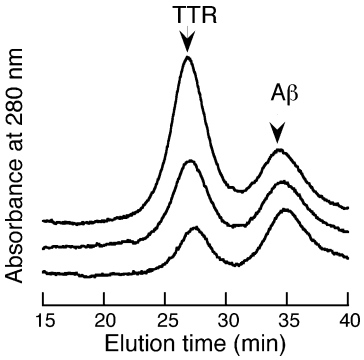

FIGURE 2: Size exclusion chromatograms of Aβ−TTR samples. The concentration of Aβ is 140 μM in all the samples. From bottom to top, TTR concentration is 1, 2, or 3.3 μM. Absorbance was detected at 280 nm. The arrows indicate the elution times of TTR and Aβ alone.

analyzed, there was no significant shift in peak elution times. From analysis of the peak areas we determined that the fraction of aggregated Aβ was not changed, nor was there any detectable loss of TTR to the Aβ aggregates. These data demonstrate that TTR does not affect the distribution of Aβ between aggregated and nonaggregated forms, nor is TTR stably bound to Aβ monomer or aggregates to any measurable extent under these experimental conditions.

More quantitative information on the size of Aβ aggregates in the presence of TTR was obtained by static and dynamic light scattering. Representative multiangle scattering data for Aβ alone and with TTR, taken 20 h after sample preparation, are shown in Figure 3A in the Zimm format and in Figure 3B in the Kratky format. For Aβ alone and with 1 μM TTR, the aggregate size is sufficiently large to obtain information on particle shape and the shape of the curve is consistent with a semiflexible chain morphology. Therefore, the data in Figure 3B were fitted to eqs 2 and 3 to determine M_w, L_c, and l_k, and R_g was calculated from eq 4. For the samples containing 2 or 3.3 μM TTR, scattering was weaker and the angular dependence was insufficient to obtain particle morphology information. For these samples, the low angle (20−50°) data were fitted to eq 2 to estimate M_w and R_g. Results are summarized in Table 1. Also included in Table 1 is the average hydrodynamic radius R_{hz} measured by dynamic light scattering. To check for consistency between multiangle static scattering measurements and dynamic scattering data, we calculated R_h from L_c and l_k and included these results in Table 1. The calculated values of R_h agree with measured values within error, providing further support for use of the semiflexible model and indicating consistency between static and dynamic light scattering measurements.

From the data in Table 1 we conclude that TTR strongly decreases the average size of Aβ aggregates, in a dose-dependent manner. Inhibition is substantial even at TTR:Aβ ratios well below a stoichiometric (1:1) ratio. Addition of just 1 μM TTR resulted in a ∼10-fold decrease in M_w; a further 10-fold decrease was obtained if the TTR concentration was increased to 3.3 μM. Substantial decreases in R_g and R_{hz} were also observed. (Because R_g is more heavily weighted toward larger aggregates than is R_{hz}, R_g is much more sensitive to the presence of a few large aggregates. This might explain why R_{hz} but not R_g decreases as TTR concentration increases from 2 to 3.3 μM.)

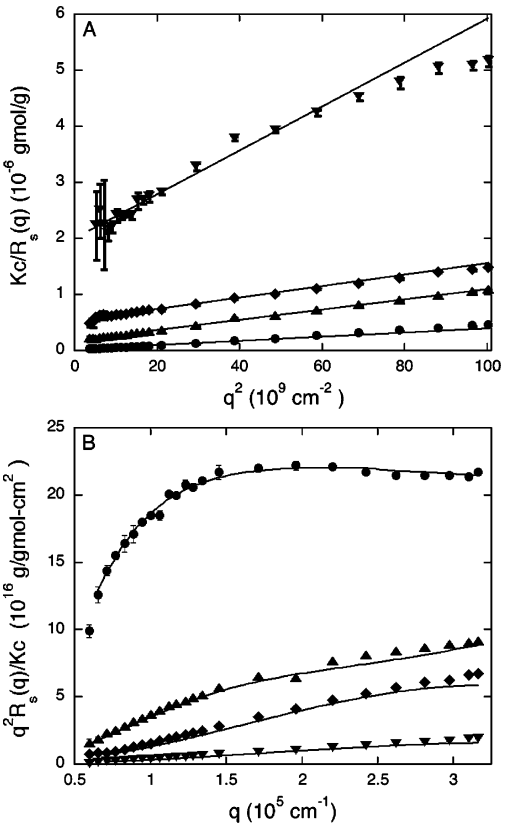

FIGURE 3: Zimm plots (A) and Kratky plots (B) of static light scattering intensity data of Aβ alone (●), or with TTR at 1 μM (▲), 2 μM (◆), or 3.3 μM (▼). The concentration of Aβ is 140 μM in all the samples. Data were collected 20 h after sample preparation. (A) Lines indicate linear regression fit of low-angle data to eq 1. (B) Lines indicate nonlinear regression fit of eqs 2 and 3 to the data.

Table 1: Size Characteristics of Aβ−TTR Mixtures, Obtained from Static and Dynamic Light Scattering Data Taken 20 h after Sample Preparation[a]

TTR (μM)	M_w (10^6 Da)	L_c (nm)	l_k (nm)	R_g (nm)	R_{hz} (DLS) (nm)	R_h (calc) (nm)
0	50 ± 20	2600 ± 800	100 ± 30	200 ± 40	99	120 ± 50
1	5 ± 0.3	440 ± 20	280 ± 50	98 ± 5	53	49 ± 2
2	1.86 ± 0.07	na	na	76 ± 5	37	na
3.3	0.5 ± 0.05	na	na	80 ± 20	18	na

[a] All samples contained 140 μM (0.6 mg/mL) Aβ. For samples containing 0 or 1 μM (0.06 mg/mL) TTR, the weight-average molecular weight M_w, the average contour length L_c, and the Kuhn length l_k were obtained from fitting the data in Figure 3B to eqs 2 and 3, using $P(q)$ for a semiflexible chain. R_g was calculated from L_c and l_k per eq 4. For samples containing 2 or 3.3 μM TTR, M_w and the z-average radius of gyration R_g were obtained by linear least-squares regression of low angle (50° or less) data shown in Figure 3A to eq 1. R_{hz} (DLS) was measured by dynamic light scattering. R_h (calc) was calculated from L_c and l_k using theoretical expressions (*28*) to check for consistency. Errors are 95% confidence intervals, based on fitting one representative set of multiangle light scattering data.

M_w is the weight-averaged molecular weight of all the species in the solution, $M_w = \sum w_i M_i$, where w_i and M_i are, respectively, the weight fraction and molecular weight of species i. The SEC data indicate that TTR neither aggregates nor dissociates into monomer in the presence of Aβ, nor is it stably incorporated into the Aβ aggregates. Also, from SEC we estimate that 67% of Aβ is monomer or dimer, while

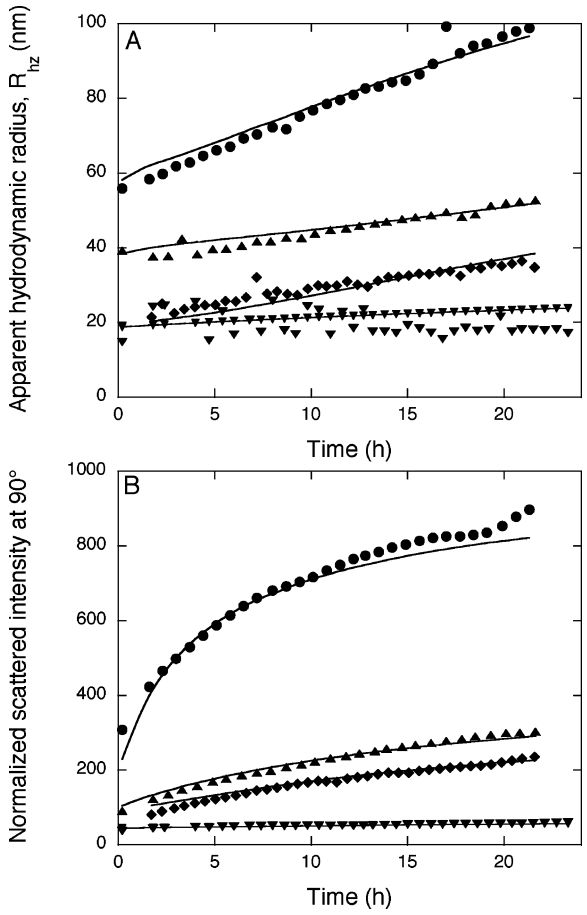

FIGURE 4: Hydrodynamic radius R_{hz} (A) and scattering intensity at 90° angle I_{90} (B) for Aβ alone (●), or with TTR at 1 μM (▲), 2 μM (◆), or 3.3 μM (▼). The concentration of Aβ is 140 μM in all the samples. The solid lines indicate the best fit of the kinetic model to the combined data. To enhance readability, only every fifth data point is shown.

33% of the Aβ peptide is incorporated into large aggregates. Given these data, and the fact that the molecular weights of Aβ monomers/dimers are much smaller than that of Aβ aggregates, we estimate M_{agg} as

$$M_{agg} \approx \frac{M_w - w_{TTR}M_{TTR}}{w_{agg}} \quad (6)$$

where w_{agg} and w_{TTR} are the weight fraction of aggregates and TTR, and M_{agg} and M_{TTR} are the molecular weights of aggregates and TTR, respectively. From eq 6 and the data in Table 1, we obtained estimates that $M_{agg} \sim 150$ MDa, 17 MDa, 7 MDa, and 2 MDa for Aβ aggregates in the presence of 0, 1, 2, and 3.3 μM TTR, respectively. This calculation demonstrates that the measured reduction in average M_w is indicative of a real reduction in the size of the Aβ aggregates and is not simply a dilution effect of TTR. The aggregate linear density, ρ_{lin}, obtained by dividing M_{agg} by L_c, is ~58 kDa/nm for Aβ alone and ~39 kDa/nm for Aβ + 1 μM TTR. These linear densities correspond to average fibril diameters (*24*) of roughly 12 and 10 nm, respectively, typical for amyloid fibril diameters.

Effect of TTR on the Aβ Aggregation Kinetics. Next, we measured the effect of TTR on the kinetics of aggregation of Aβ by following R_{hz} and I_{90} versus time (Figure 4).

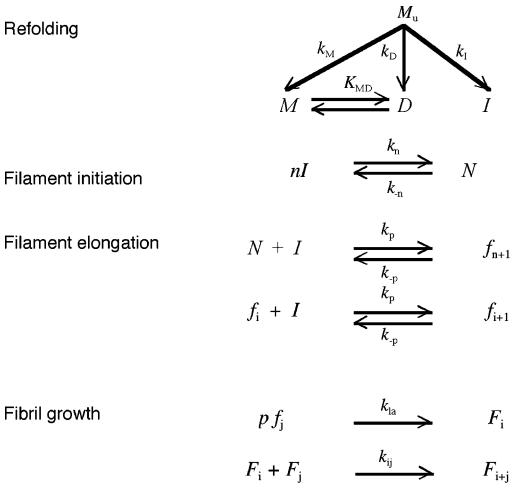

Model parameters	
K_{MD}	*M-D* equilibrium (μM^{-1})
k_M/k_I	Relative rate of *M* to *I* formation from M_u (μM)
k_D/k_I	Relative rate of *D* to *I* formation from M_u (—)
k_n/k_p	Relative rate of filament initiation versus filament elongation (μM^{-4})
k_{la}	Rate of lateral alignment of filaments ($\mu M^{-2}h^{-1}$)
$\delta\omega_{fib}$	Factor for base rate of end-to-end association of fibrils (cm-rad)

FIGURE 5: Aβ aggregation kinetic model developed by Pallitto and Murphy (*24*).

Roughly, R_{hz} scales with the average aggregate length and I_{90} scales with the average aggregate molecular weight. By either measure, we observed that both the initial size (data taken ~10 min after sample preparation) and the rate of growth decreased with increasing TTR concentration. At the highest TTR concentration tested (3.3 μM), there was virtually no increase in size over time. As a negative control, 10 μM TTR was stable and showed no sign of aggregation over a 24 h period (data not shown).

To obtain greater insight into the mechanism of inhibition of Aβ aggregation by TTR, the data were analyzed quantitatively using a previously described mathematical model of Aβ aggregation kinetics (*24*). The model is shown schematically in Figure 5, along with a listing of the key model parameters. Briefly, unstructured monomers M_u (in 8 M urea) are hypothesized to quickly "refold" upon dilution into PBSA into either stable monomers/dimers, M/D, or unstable dimeric intermediates, I. The intermediate I rapidly and cooperatively assembles to nuclei, N, to initiate formation of thin filaments, f. Filaments grow linearly by continuous addition of I. Cooperative lateral association of filaments results in formation of fibrils, F. Further elongation of fibrils by end-to-end association is allowed.

TTR did not affect the partitioning of Aβ between nonaggregated and aggregated species, as shown by the SEC data (Figure 2). Therefore, we used previously determined values (*24*) for the model parameters associated with the initial dilution step: K_{MD}, k_M/k_I, and k_D/k_I. The kinetic data (Figure 4) were used to obtain the best fit values for those model parameters associated with aggregate growth, i.e., filament initiation and elongation (k_p/k_n), fibril formation by lateral association (k_{la}) and fibril growth by end-to-end

Table 2: Fitted Values for Model Parameters[a]

TTR concn (μM)	k_p/k_n ($10^{10}\mu M^4$)	k_{la} ($10^{-2}\,\mu M^{-2}\,h^{-1}$)	$\delta\omega_{fib}$ (10^{-8} cm-rad)
0	3 ± 2	188 ± 3	13.8 ± 0.2
1.0	0.7 ± 0.1	32.7 ± 0.7	1.8 ± 0.1
2.0	0.2 ± 0.1	20.6 ± 0.7	0.75 ± 0.06
3.3	0.03 ± 0.02	0.25 ± 0.06	nd[b]

[a] The kinetic light scattering data were fitted to the model sketched in Figure 5 and discussed in ref *24*. All samples contained 140 μM Aβ and the indicated concentration of TTR. Parameter errors indicate 95% confidence intervals, based on fitting one representative set of kinetic data. [b] Not determined. With 3.3 μM TTR in 140 μM Aβ solution, there was almost no increase in R_h and I_{90} over time. Hence $\delta\omega_{fib} \sim 0$.

association ($\delta\varpi_{fib}$). Model calculations are plotted alongside the experimental data in Figure 4. Fitted parameter values are summarized in Table 2. The model captured the growth of Aβ aggregates in the presence of TTR reasonably well. The ratio k_p/k_n, which represents the ratio of elongation of existing filaments relative to formation of new ones, was reduced several-fold upon addition of TTR (Table 2). A reduction in the relative elongation rate is consistent with the decrease in length of Aβ aggregates observed in TEM images (Figure 1) and by SLS (Table 1). The values of k_{la} and $\delta\varpi_{fib}$, which characterize rates of lateral association of filaments and end-to-end growth of fibrils, respectively, were also reduced considerably (Table 2). Taken together, the data indicate that TTR inhibits Aβ aggregation by suppressing growth of pre-existing aggregates rather than by preventing the initial Aβ self-association.

Binding Affinity of Aβ and TTR. As shown in Figure 2, we observed no evidence for a strong stable association between TTR and Aβ by SEC, yet light scattering and electron microscopy clearly showed that TTR strongly suppressed Aβ aggregation (Figures 1, 3, and 4). We speculated that we might be able to detect evidence of Aβ−TTR association by probing for changes in intrinsic tryptophan fluorescence. The wavelength at which maximum Trp fluorescence is observed depends on solvent exposure, while Trp fluorescence intensity can be quenched by lysine, tyrosine, glutamine, and asparagine (*30*). There are two tryptophans in a TTR monomer, Trp41 and Trp79; approximately one-third of the side chain of Trp41 is exposed to solvent while that of Trp79 is completely buried (*31*). Trp41 is by far the major contributor to TTR's fluorescence signal (*32*). Aβ has no tryptophan residue. We therefore reasoned that binding of Aβ to TTR might be detectable if Aβ quenched Trp41 fluorescence.

Samples of 1 μM TTR mixed with excess Aβ (21, 42, and 84 μM) were excited at 290 nm, and Trp emission spectra were collected. Aβ alone produced no emission spectra, as expected. Emission spectra of TTR alone and with Aβ showed decreasing fluorescence intensity with increasing Aβ concentration (Figure 6A), but no shift in the wavelength for maximum fluorescence. When TTR was mixed with non-amyloidogenic fragments Aβ(1−11) and Aβ(12−28), no quenching was detected (data not shown). Thus, we concluded that full length Aβ quenches Trp fluorescence in TTR. Analysis of fluorescence intensity data using the Stern−Volmer equation (Figure 6B) yielded an estimate of $K_S = 2300 \pm 100\ M^{-1}$, indicating a weak association.

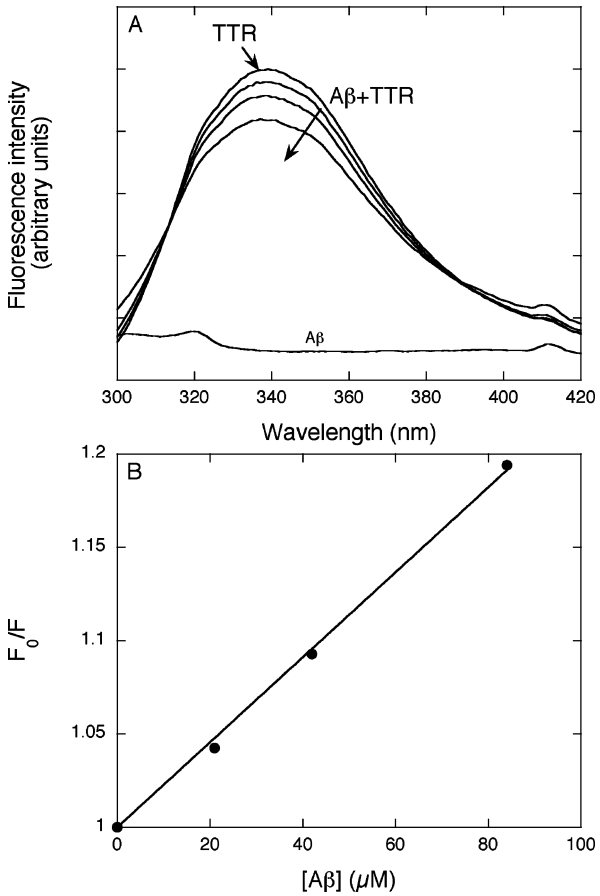

FIGURE 6: (A) Tryptophan fluorescence emission spectra for 1 μM TTR alone and with increasing Aβ (21, 42, and 84 μM). Excitation was at 290 nm. (B) Stern−Volmer plot of the fluorescence intensity at 339 nm versus Aβ concentration. The solid line is the linear regression fit of eq 5 to the data.

DISCUSSION

Deposition of Aβ amyloid fibrils is one of several defining features of AD, and a substantial body of evidence supports the "amyloid cascade hypothesis" in which Aβ aggregation is causally linked to neuronal loss. Although it is fairly well-established that conversion of monomeric and unstructured Aβ into β-sheet aggregates is required for gain of toxicity, it remains controversial whether soluble oligomeric aggregates or fully formed fibrils are the dominant toxic species (*33*). In the absence of a natural animal model for human AD, attempts have been made to generate transgenic mice with the disease phenotype. Mice expressing human APP with the Swedish mutation (APP_{Sw}) produce significant quantities of Aβ and develop numerous amyloid plaques but, surprisingly, lack the classical paired helical filaments and neuronal cell loss prevalent in the human disease (*5*, *6*). This finding has led some to question the validity of the amyloid cascade hypothesis. Stein and Johnson hypothesized that APP_{Sw} mice are models, not of AD, but of protection from the disease. In DNA microarray and immunostaining studies, they demonstrated conclusively that APP_{Sw} mice respond to APP overexpression by upregulating biosynthesis of TTR several-fold, likely in response to increased production of sAPPα (*7*, *8*). They further demonstrated that 50 μM Aβ caused significant cell death in hippocampal brain slices, and that 3 μM TTR completely abrogated this toxicity (*8*). Additionally, anti-TTR antibodies reversed the neuroprotec-

tive effect of sAPPα-induced increases in TTR synthesis (*8*). In independent studies, other researchers identified TTR as a protein capable of binding to Aβ (*20*, *21*), leading Schwarzman and co-workers to propose that sequestration of Aβ by TTR inhibited its aggregation and toxicity (*19*).

Given the significance of Aβ−TTR association, we investigated the effect of TTR on the morphology of Aβ aggregates and the kinetics of aggregation. TEM and light scattering analysis showed that TTR inhibited Aβ aggregation dramatically. Substantial reductions in the length of amyloid fibrils and in the rate of growth were observed even at ∼100-fold Aβ molar excess. Addition of more TTR repressed the Aβ aggregation further, demonstrating a strong concentration-dependent response. Interestingly, the aggregates observed under EM were not amorphous but retained a linear morphology. This suggests that TTR suppresses growth of aggregates but not initial assembly. Further support for this hypothesis is provided by the SEC data showing that TTR did not alter the distribution of Aβ between aggregated and nonaggregated species (Figure 2).

To further probe the mechanism of action of TTR, we analyzed Aβ aggregation kinetics using a previously described mathematical model (*24*). (We note that our model describes the aggregation process prior to precipitation of insoluble fibrils.) By fitting the data to the model we determined that TTR decreased k_p/k_n, indicating a reduction in filament elongation relative to initiation (Figure 4 and Table 2). The net effect of this change is a decrease in the length of aggregates. TTR also caused a decrease in k_{la}, a parameter describing the rate of lateral association of filaments to fibrils (Table 2). Given this analysis, we hypothesize that TTR binds preferentially to growing Aβ filaments, inhibiting elongation as well as lateral alignment into fibrils. Further indirect support for the notion that TTR binds preferentially to Aβ aggregates rather than nonaggregated peptide is supplied by Trp fluorescence quenching experiments, in which we showed that full-length Aβ but not nonaggregating Aβ fragments (Aβ(1−11) and Aβ(12−28)) quench TTR's Trp fluorescence.

Although the interaction of TTR and Aβ has been observed by several groups, measurement of the binding affinity has not been reported to our knowledge. We observed that Aβ quenched TTR Trp fluorescence in a concentration-dependent manner. From application of the Stern−Volmer equation we calculated an association constant $K_S \sim 2300 \pm 100\ M^{-1}$. This relatively weak binding may explain why stable TTR−Aβ complexes were not detected by SEC, since the samples become diluted during chromatography. This calculated value of K_S is based on the molar concentration of Aβ monomers. If, however, TTR binds only to Aβ aggregates, the effective molar concentration of aggregates is much lower and therefore the effective association constant is much higher. If the higher molecular weight of Aβ aggregates is accounted for, the estimated K_S increases by ∼3 orders of magnitude.

There are two tryptophans in a TTR monomer, Trp41 and Trp79. According to the crystal structure of human TTR (PDB code 1DVQ), the side chain of Trp41 is partially exposed while that of Trp79 is buried. Most of the Trp fluorescence in TTR can be attributed to Trp41 (data not shown) (*32*). Since quenching is observed, it is reasonable to postulate that the region near Trp41 is involved in binding to Aβ aggregates. This result is consistent with data reported by Schwarzman et al. (*23*) that peptide fragments corresponding to residues 37−43 and 30−60 of TTR bind to Aβ. Alternatively, quenching of Trp41 could be due to Aβ-induced changes in TTR structure rather than direct interaction between a side chain in Aβ and Trp41.

TTR concentration in plasma is 3−7 μM, while in CSF its concentration is ∼0.3 μM (*19*). Aβ concentration in CSF is about 3 nM (*34*), although the local concentration in and near amyloid deposits could be much higher. Thus, in our *in vitro* experiments the TTR concentration reflected the *in vivo* situation but the Aβ concentration was much higher than what would typically be observed in physiological fluids. Our data suggests that TTR, whether by design or accident, might patrol the CSF and suppress further growth of nascent Aβ aggregates. Through this action, TTR may inhibit accumulation of toxic aggregates and prevent or delay neuronal death. TTR synthesis is upregulated by sAPPα (*7*), and TTR concentration in the CSF of patients with AD is lower than that in age-matched controls (*14*, *15*). It is tempting to speculate that even small imbalances in APP proteolysis, in which α-secretase activity is decreased relative to β- and γ-secretase activities, could lead to an increase in Aβ synthesis and a corresponding decrease in sAPPα and, therefore, TTR synthesis, leading to escape of Aβ aggregation from TTR's control. This scenario suggests therapeutic strategies based on drugs that restore normal CSF levels of TTR, or compounds that mimic TTR's sequestering ability. The latter strategy requires further molecular-level information about the means by which TTR interacts with Aβ aggregates and suppresses their further growth.

REFERENCES

1. Hardyr, J. A., and Higgins, G. A. (1992) Alzheimer's disease: the amyloid cascade hypothesis, *Science 256*, 184−185.
2. Kang, J., Lemaire, H. G., Unterbeck, A., Salbaum, J. M., Masters, C. L., Grzeschik, K. H., Multhaup, G., Beyreuther, K., and Muller-Hill, B. (1987) The precursor of Alzheimer's disease amyloid A4 protein resembles a cell-surface receptor, *Nature 325*, 733−736.
3. Goodman, Y., and Mattson, M. P. (1994) Secreted forms of β-amyloid precursor protein protect hippocampal neurons against amyloid β -peptide-induced oxidative injury, *Exp. Neurol. 128*, 1−12.
4. Thornton, E., Vink, R., Blumberg, P. C., and van den Heuval, C. (2006) Soluble amyloid precursor protein α reduces neuronal injury and improves functional outcome following diffuse traumatic brain injury in rats, *Brain Res. 1094*, 38−46.
5. Kawarabayashi, T., Younkin, L. H., Saido, T. C., Shoji, M., Ashe, K. H., and Younkin, S. G. (2001) Age-dependent changes in brain, CSF, and plasma amyloid (beta) protein in the Tg2576 transgenic mouse model of Alzheimer's disease, *J. Neurosci. 21*, 372−381.
6. Irizarry, M. C., McNamara, M., Fedorchak, K., Hsiao, K., and Hyman, B. T. (1997) APP_{Sw} transgenic mice develop age-related Abeta deposits and neuropil abnormalities, but no neuronal loss in CA1, *J. Neuropathol. Exp. Neurol. 56*, 965−973.
7. Stein, T. D., and Johnson, J. A. (2002) Lack of neurodegeneration in transgenic mice overexpressing mutant amyloid precursor protein is associated with increased levels of transthyretin and the activation of cell survival pathways, *J. Neurosci. 22*, 7380−7388.
8. Stein, T. D., Anders, N. J., DeCarli, C., Chan, S. L., Mattson, M. P., and Johnson, J. A. (2004) Neutralization of transthyretin reverses the neuroprotective effects of secreted amyloid precursor protein (APP) in APP_{Sw} mice resulting in tau phosphorylation and loss of hippocampal neurons: support for the amyloid hypothesis, *J. Neurosci. 24*, 7707−7717.
9. Hamilton, J. A., and Benson, M. D. (2001) Transthyretin: a review from a structural perspective, *Cell. Mol. Life Sci. 58*, 1491−1521.

10. Lashuel, H. A., Lai, Z., and Kelly, J. W. (1998) Characterization of the transthyretin acid denaturation pathways by analytical ultracentrifugation: implications for wild-type, V30M, and L55P amyloid fibril formation, *Biochemistry 37*, 17851−17864.
11. Westermark, P., Sletten, K., Johansson, B., and Cornwell, G. G. (1990) Fibril in senile systemic amyloidosis is derived from normal transthyretin, *Proc. Natl. Acad. Sci. U.S.A. 87*, 2843−2845.
12. Saraiva, M. J., Birken, S., Costa, P. P., and Goodman, D. S. (1984) Amyloid fibril protein in familial amyloidotic polyneuropathy, Portuguese type. Definition of molecular abnormality in transthyretin (prealbumin), *J. Clin. Invest. 74*, 104−119.
13. Riisoen, H. (1988) Reduced prealbumin (transthyretin) in CSF of severely demented patients with Alzheimer's disease, *Acta Neurol. Scand. 78*, 455−459.
14. Serot, J. M., Christmann, D., Dubost, T., and Couturier, M. (1997) Cerebrospinal fluid transthyretin: aging and late onset Alzheimer's disease, *J. Neurol., Neurosurg. Psychiatry 63*, 506−508.
15. Castano, E. M., Roher, A. E., Esh, C. L., Kokjohn, T. A., and Beach, T. (2006) Comparative proteomics of cerebrospinal fluid in neuropathologically-confirmed Alzheimer's disease and nondemented elderly subjects, *Neurol. Res. 28*, 155−163.
16. Li, M. D., Kane, J. K., Matta, S. G., Blaner, W. S., and Sharp, B. M. (2000) Nicotine enhances the biosynthesis and secretion of transthyretin from the choroid plexus in rats: implications for beta-amyloid formation, *J. Neurosci. 20*, 1318−1323.
17. Tang, Y. P., Haslam, S. Z., Conrad, S. E., and Sisk, C. L. (2004) Estrogen increases brain expression of the mRNA encoding transthyretin, an amyloid beta scavenger protein, *J. Alzheimer's Dis. 6*, 413−420; discussion 443−449.
18. Link, C. D. (1995) Expression of human beta-amyloid peptide in transgenic *Caenorhabditis elegans*, *Proc. Natl. Acad. Sci. U.S.A. 92*, 9368−9372.
19. Schwarzman, A. L., Gregori, L., Vitek, M. P., Lyubski, S., Strittmatter, W. J., Enghilde, J. J., Bhasin, R., Silverman, J., Weisgraber, K. H., Coyle, P. K., Zagorski, M. G., Talafous, J., Eisenberg, M., Saunders, A. M., Roses, A. D., and Goldgaber, D. (1994) Transthyretin sequesters amyloid beta protein and prevents amyloid formation, *Proc. Natl. Acad. Sci. U.S.A. 91*, 8368−8372.
20. Schwarzman, A. L., and Goldgaber, D. (1996) Interaction of transthyretin with amyloid beta-protein: binding and inhibition of amyloid formation, *Ciba Found. Symp. 199*, 146−160; discussion 160−164.
21. Tsuzuki, F., Fukatsu, R., Hayashi, Y., Yoshida, T., Sasaki, N., Takamaru, Y., Yamaguchi, H., Tateno, M., Fujii, N., and Takahata, N. (1996) Amyloid β-protein and transthyretin, sequestrating protein colocalize in normal human kidney, *Neurosci. Lett. 222*, 163−166.
22. Schwarzman, A. L., Tsiper, M., Wente, H., Wang, A., Vitek, M. P., Vasiliev, V., and Goldgaber, D. (2004) Amyloidogenic and anti-amyloidogenic properties of recombinant transthyretin variants, *Amyloid 11*, 1−9.
23. Schwarzman, A. L., Tsiper, M., Gregori, L., Goldgaber, D., Frakowiak, J., Mazur-Kolecka, B., Taraskina, A., Pcheina, S., and Vitek, M. P. (2005) Selection of peptides binding to the amyloid β protein reveals potential inhibitors of amyloid formation, *Amyloid 12*, 199−209.
24. Pallitto, M. M., and Murphy, R. M. (2001) A mathematical model of the kinetics of beta-amyloid fibril growth from the denatured state, *Biophys. J. 81*, 1805−1822.
25. Lowe, T. L., Strzelec, A., Kiessling, L. L., and Murphy, R. M. (2001) Structure-function relationships for inhibitors of beta-amyloid toxicity containing the recognition sequence KLVFF, *Biochemistry 40*, 7882−7889.
26. Burchard, W. (1983) Static and dynamic light scattering from branched polymers and biopolymers, *Adv. Polym. Sci. 48*, 4−124.
27. Shen, C. L., Fitzgerald, M. C., and Murphy, R. M. (1994) Effect of acid predissolution on fibril size and fibril flexibility of synthetic beta-amyloid peptide, *Biophys. J. 67*, 1238−46.
28. Yamakawa, H., and Fujii, M. (1973) Translational friction coefficient of wormlike chains, *Macromolecules 6*, 407−415.
29. Lakowicz, J. R. (1983) *Principles of Fluorescence Spectroscopy*, p 260, Plenum Press, New York.
30. Chen, Y., and Barkley, M. D. (1998) Toward understanding tryptophan fluorescence in proteins, *Biochemistry 37*, 9976−9982.
31. Quintas, A., Saraiva, M. J., and Brito, R. M. (1999) The tetrameric protein transthyretin dissociates to a non-native monomer in solution. A novel model for amyloidogenesis, *J. Biol. Chem. 274*, 32943−32949.
32. Lai, Z., Colon, W., and Kelly, J. W. (1996) The acid-mediated denaturation pathway of transthyretin yields a conformational intermediate that can self-assemble into amyloid, *Biochemistry 35*, 6470−6482.
33. Watson, D., Castano, E., Kokjohn, T. A., Kuo, Y.-M., Lyubchenko, Y., Pinsky, D., Connolly, E. S., Esh, C., Luehrs, D. C., Stine, W. B., Rowse, L. M., Emmerling, M. R., and Roher, A. E. (2005) Physicochemical characteristics of soluble oligomeric Aβ and their pathologic role in Alzheimer's disease, *Neurol. Res. 27*, 869−881.
34. Price, J. M., Chi, X., Hellermann, G., and Sutton, E. T. (2001) Physiological levels of β-amyloid induce cerebral vessel dysfunction and reduce endothelial nitric oxide production, *Neurol. Res. 23*, 506−512.

BI0618520